

Simple method to construct flat-band lattices

Luis Morales-Inostroza and Rodrigo A. Vicencio*

*Departamento de Física and MSI-Nucleus on Advanced Optics, Center for Optics and Photonics, Facultad de Ciencias,
Universidad de Chile, Santiago 7800003, Chile*

(Received 14 July 2016; published 18 October 2016)

We develop a simple and general method to construct arbitrary flat-band lattices. We identify the basic ingredients behind zero-dispersion bands and develop a method to construct extended lattices based on a consecutive repetition of a given miniarray. The number of degenerated localized states is defined by the number of connected miniarrays times the number of modes preserving the symmetry at a given connector site. In this way, we create one or more (depending on the lattice geometry) complete degenerated flat bands for quasi-one- and two-dimensional systems. We probe our method by studying several examples and discuss the effect of additional interactions such as anisotropy or nonlinearity. We test our method by studying numerically a ribbon lattice using a continuous description.

DOI: [10.1103/PhysRevA.94.043831](https://doi.org/10.1103/PhysRevA.94.043831)

I. INTRODUCTION

Lattices or extended periodic systems constitute a central framework for several areas of research. For example, in solid-state physics periodic lattices are a fundamental starting point [1], where many general predictions have been made without a direct experimental observation. In recent decades, photonic lattices have emerged as key experimental setups to study most of the predicted electronic properties, due to a direct observation of the optical wave function using a simple CCD camera [2]. In this context, Anderson localization [3] was directly observed first in two-dimensional (2D) waveguide arrays [4] and then also in one-dimensional (1D) lattices [5]. In this case, the energy is trapped due to consecutive destructive interference from randomly distributed scatters (sites or waveguides). Before this very fundamental observation, localization resulting as a balance between discreteness (diffraction) and nonlinearity (self-focusing) was observed in 1D [6–8] and 2D [9,10] lattices. Nonlinear localized modes of this nature are known as discrete solitons or intrinsic localized modes [11] and the conditions for existence and stability, in diverse contexts, are nowadays well understood [12]. The nonlinearity and larger intensities create effective defect regions, where the trapping potential changes locally. In this way, waves naturally get trapped at deeper potential wells. In the nonlinear case, this occurs in a perfectly periodic lattice; however, this type of phenomenon can also be observed in a linear regime by directly inserting a linear defect into a homogeneous system [13,14]. Exponentially decaying localized modes are obtained in both linear and nonlinear cases, depending on the effective strength of the induced defect. Therefore, these modes are not compact and high localization demands a very strong effective disturbance.

Another interesting way to induce localization on a lattice originates from the understanding of the linear properties of a given unconventional array. In standard periodic systems (e.g., square, hexagonal, or honeycomb lattices) the linear spectrum is always dispersive (except for some k -space points where the derivative becomes locally zero). As a result, when exciting the lattice, for example, using a single-site

excitation, a set of linear extended modes, with different spatial frequencies, will be excited and waves will propagate without spatial coherence across the lattice, generating a multimode interference pattern [15]. Therefore, stationary localized patterns will be not observed for perfectly periodic linear standard lattices and the energy will diffuse only [2]. However, by carefully selecting the geometry of the lattice, a different kind of linear spectrum can be obtained. A flat-band (FB) (unconventional) lattice possesses a unique linear spectrum. In these quasi-1D or 2D systems, a complete band (not only a section of it) is completely flat, implying zero dispersion and not diffraction at all for the states belonging to this band. Diamond [16], stub [17], sawtooth [18,19], kagome [20,21], or Lieb [22–24] lattices are some examples of recent explored FB systems, in diverse physical contexts. These examples show the diversity of fabrication techniques and impressive possibilities for creating, in principle, any wished lattice. In all these geometries, a FB is composed of a large set of degenerated localized linear modes, all of them propagating coherently along the lattice. Moreover, these states occupy only a few lattice sites being exactly compact (zero tail), in a perfectly periodic linear lattice. This implies that the localization is always perfect and it does not depend on any external parameter. The special geometry of FB systems generates consecutive phase cancellations that effectively reduce the excited region to a miniarray of a given lattice. The linear combination of these localized states is thought to be important for applications in all-optical imaging transmission [25,26], as a secure and compact mechanism of transporting information at a very low level of power.

There have been several attempts to find a simple method to construct FB lattices [27–30]. However, we have not found a direct, simple, and general method to create any wished FB system with given specific features (e.g., having several zero-dispersion bands). For example, Ref. [28] starts from a given 2D or 3D lattice and constructs partial line graphs without much connection with the physics of the sublattices, which is of major relevance in our method. In Ref. [31] Hyrkäs *et al.* describe a collection of FB lattices to study bosons and fermions dynamics. They briefly mention that an important condition is that the wave function may be zero at some connecting sites, in order to make impossible

*rvicencio@uchile.cl

the transport across the lattice. It is important to notice that this is an important requirement, but it is not complete. It is possible to excite any lattice with a profile having zero amplitudes at some connecting sites; however, the energy could nevertheless diffuse and the FB will be not exclusively excited. To observe localization, as a result of the excitation of any FB, a mandatory condition is to excite the lattice by one of the modes of a given miniarray (or a linear combination of them) that has zero amplitude at the connecting sites. The additive destructive interference will make possible the cancellation of the amplitude at the connecting sites and the transport will be just forbidden.

In this work we identify the key ingredients to construct arbitrary lattices possessing one or more flat bands, focusing on the consecutive addition of miniarrays to form an extended lattice. Our method is based on the knowledge of the fundamental linear modes belonging to a given miniarray, in order to ensure the cancellation of phases at connector sites. The existence of a linear mode satisfying this condition constitutes a proof to guarantee the existence of a flat band, which is composed of compact localized states. Different systems in quasi-one- and two-dimensions are generated with one or more flat bands (it is straightforward to extend our method to three dimensions as well). Additionally, we also show that it is possible to use our method to construct aperiodic systems having a set of compact modes forming a full FB. Extra considerations, for example, anisotropy, next-nearest-neighbor interactions, or local nonlinearity, are also discussed. Finally, we study a ribbon lattice using a continuous model where we test our discrete predictions in a more realistic configuration.

II. GENERAL MODEL

Focusing on written and induced waveguide lattices [2], we model the propagation of light in weakly coupled systems using a discrete linear Schrödinger equation. In this model, a given waveguide mode weakly interacts with its close neighbors due to an evanescent interaction. The amplitude of the mode at the \vec{n} th waveguide position is given by $\psi_{\vec{n}}$ and its dynamical evolution is simply modeled as

$$-i \frac{d\psi_{\vec{n}}}{dz} = \epsilon_{\vec{n}} \psi_{\vec{n}} + \sum_{\vec{m} \neq \vec{n}} V_{nm} \psi_{\vec{m}}, \quad (1)$$

where z is the propagation coordinate (in other contexts, it corresponds to time [2,12]), $\epsilon_{\vec{n}}$ corresponds to the propagation constant at the \vec{n} th site (if the lattice is homogeneous, we simply set $\epsilon_{\vec{n}} = 0$, without loss of generality), and V_{nm} describes the coupling interaction between the \vec{n} th and \vec{m} th sites. When constructing the lattice, these coefficients define all the linear interactions between close sites, according to a given lattice geometry. In fact, as we will discuss below, some FBs also survive when including next-nearest-neighbor interactions, of course, taking into account the exponentially decaying tendency of coupling constants with respect to separation distance [32]. For some FB lattices the anisotropy or next-nearest-neighbor interactions destroy the flatness of the band. However, we will show that our method allows the construction of more robust systems, which is important to

observe the FB phenomenology in real experiments [16,19,21–23,26,33].

In general, the linear properties of any periodic system are contained in the definition of V_{nm} coefficients. We solve the stationary problem by using a plane-wave (Bloch) ansatz

$$\psi_{\vec{n}}(z) = A_{\vec{n}} e^{i\vec{k} \cdot \vec{n}} e^{i\beta z},$$

where \vec{k} corresponds to the lattice wave vector and β describes the longitudinal propagation constant or spatial frequency. By inserting this into the model (1), we obtain the following set of coupled stationary equations:

$$\beta(\vec{k}) A_{\vec{n}} = \sum_{m \neq n} V_{nm} A_{\vec{m}} e^{i\vec{k} \cdot (\vec{m} - \vec{n})}. \quad (2)$$

By solving this eigenvalue problem, we obtain the linear spectrum of a given lattice according to the interactions defined by V_{nm} . All the coupling interactions between close waveguides are explicitly described in this term. (Throughout this work we consider a constant spatial period of $a = 1$, in order to simplify the expressions.) The number of sites per unitary cell defines the number of different amplitudes $A_{\vec{n}}$ to be considered. For example, in a system with three sites per unit cell (e.g., stub, Lieb, or kagome lattices), we require three different amplitudes to characterize the linear properties of the system having three linear bands.

III. TWO-SITE CASE

Let us start with the simplest possible miniarray: a dimer [see Fig. 1(a), left]. This basic system describes two close waveguides interacting via a coupling coefficient V . A dimer possesses two linear stationary modes $A_1 = A_2$ and $A_1 = -A_2$ [symbolic notation $\{+, +\}$ and $\{+, -\}$, respectively], as shown in Fig. 1(a), right (for simplicity, we do not include any mode normalization in the text). The frequencies of these modes are $\beta = V$ and $\beta = -V$, respectively. Now we increase the system size by adding a connector site in between two vertically oriented dimers [see Fig. 1(b)]. We include an

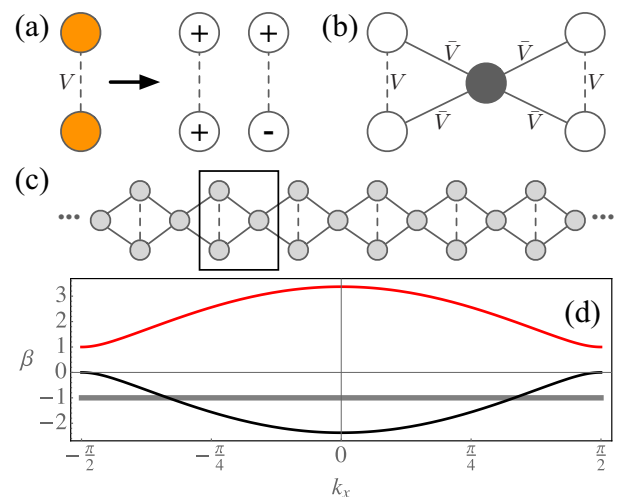


FIG. 1. (a) Dimer and its linear modes. (b) Two miniarrays connected by a connector (dark) site. (c) Rhombic lattice. (d) Linear spectrum for $V = \bar{V} = 1$.

additional coupling \bar{V} (solid line), which is determined by the specific geometry (angle and distance [32]). Immediately, we realize that the original dimer solution $\{+, -\}$, located in either of the two dimers, also corresponds to a solution (mode) of this newly composed system. For this mode, Eq. (2) reads

$$\begin{aligned}\beta \cdot 0 &= \bar{V} \cdot (A - A) = 0, \\ \beta \cdot \pm A &= V \cdot \mp A + \bar{V} \cdot 0 \Rightarrow \beta = -V.\end{aligned}$$

The phase difference between the nonzero amplitude sites allows the cancellation of the amplitude at the added connector site. The frequency of this mode, in the newly composed system, remains equal to the one of the original dimer problem ($\beta = -V$). By adding more connector sites and dimers (miniarrays), we are able to construct a full extended lattice, like the one shown in Fig. 1(c). This lattice is known as a rhombic or diamond lattice and has been recently studied experimentally in Ref. [16]. As the $\{+, -\}$ mode is still a mode in the extended system, there will be as many of these modes as the number of miniarrays (dimers) in the lattice, all of them having the same frequency $\beta = -V$. Therefore, all these modes will form a completely degenerated flat band.

We solve the linear problem (2) for the full rhombic lattice, considering the unitary cell formed by three sites [enclosed area in Fig. 1(c)], and find the bands

$$\beta(k_x) = -V, [V \pm \sqrt{V^2 + 32\bar{V}^2 \cos^2(k_x)}]/2.$$

We realize that the miniarray mode is also an exact solution of the extended system forming a full flat band at $\beta = -V$, independent of the \bar{V} value. Figure 1(d) shows the linear spectrum for this diamond lattice.

The discreteness of the system and the symmetry at the connector site equation, when considering a linear mode of the miniarray, are the keys to success to create any lattice possessing, at least, one flat band. For the previous example, assuming a $\{+, -\}$ mode (or combinations of it) as an initial condition at $z = 0$, the connector equation becomes

$$-i \frac{d\psi_{\bar{c}}}{dz} = \sum_{m \neq \bar{c}} V_{c,m} \psi_{\bar{m}}(z=0) = 0 \Rightarrow \psi_{\bar{c}}(z) = 0$$

because $\psi_{\bar{c}}(z=0) = 0$. Considering this example and extending it to other configurations, we could claim that we can construct any FB lattice by connecting any given miniarray (dimer, trimer, rhombus, etc.) via different connector sites in different directions, ensuring that the dynamical equation for this site may be strictly equal to zero. This is achieved by using a specific miniarray mode as an initial condition, which effectively allows the cancellation of phases at the connector site. In this way, we can construct a full lattice with a zero-dispersion band, where this particular miniarray mode will be a degenerated solution of the extended system. One way to ensure this is, for example, by choosing the connector sites coinciding with a node of a given mode of the miniarray. Therefore, this mode will naturally become a mode of the flat band because it will preserve the symmetry at the dynamical connector site equation. Of course, this method is not unique, but when it is successfully applied it ensures the existence of a FB.

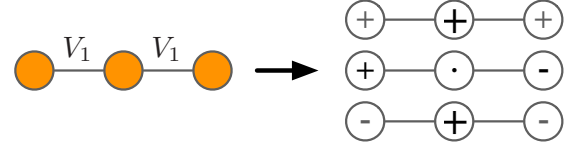


FIG. 2. Shown on the left is a three-site miniarray and on the right are linear modes.

IV. THREE-SITE CASE

Another interesting example is based on a miniarray consisting of only three sites connected in a row, as sketched in Fig. 2, left. This simple system possesses three linear stationary modes $\{+, \sqrt{2}, +\}$, $\{+, 0, -\}$, and $\{-, \sqrt{2}, -\}$, as shown in Fig. 2, right, with frequencies $\beta = \sqrt{2}, 0$, and $-\sqrt{2}$, respectively. We will show that we can use two of these modes to construct two different FB lattices.

A. Cross lattice

We start our lattice composition by selecting one of the three linear modes of the miniarray. The first mode does not present any phase oscillation. Therefore, it will not induce cancellation of transport on a given connector site, nor will it be associated with any flat band (however, this could change by assuming very rear negative coupling constants [34]). The second $\{+, 0, -\}$ mode is similar to the mode used for the dimer to create the rhombic lattice, but it has an extra zero-amplitude site at the center [see Fig. 3(a)]. So it becomes natural to use this null site to connect two miniarrays. However, if we connect a second miniarray, for example, to the right, we would end up with a system that will not preserve the symmetry of the miniarray mode and our method will simply not work (there is

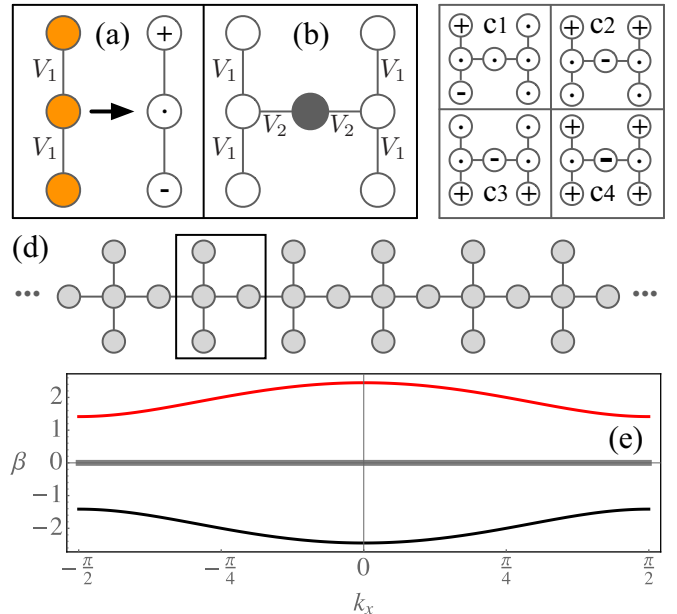


FIG. 3. (a) Three-site miniarray and one of its modes. (b) Two miniarrays connected by a connector (dark) site. (c) Four linear modes of the composed system. (d) Cross lattice. (e) Linear spectrum for $V_1 = V_2 = 1$.

a way to do it in a higher dimension, by rotating the miniarrays in 90° consecutively, obtaining a 3D FB spinelike ribbon). Therefore, we add an extra connector site in between two miniarrays as shown in Fig. 3(b), using a horizontal coupling V_2 . As we expect, the trimer $\{+, 0, -\}$ mode is also a solution of this new system [see Fig. 3(c1)] and it can be located in either of the two miniarrays or simultaneously in both. However, we realize that there is not only one FB candidate solution for this newly composed system. Interestingly, the inclusion of a connector site and the conservation of the zero amplitude site at the center of the original trimer allow the generation of new linear localized states. In Fig. 3(c2) we show a different mode, which still has a zero amplitude at the center of the three-site miniarray. This mode is exactly equal to the stub FB mode [17], although our composed system has additional sites below the central row. Due to symmetry, this mode can also be located in the bottom row as shown in Fig. 3(c3). As a consequence, another FB mode could be the one having equal amplitudes in the top and bottom rows while having a double negative amplitude at the central connector site [see Fig. 3(c4)]. This new mode preserves the zero amplitude at the miniarray center, which indeed would be the connection of the composed system to its surroundings.

In this particular case, the inclusion of an off-axis connector site adds more complexity to the original trimer miniarray. Therefore, in order to describe all the possible FB mode candidates, a new miniarray definition is required, i.e., a four-site miniarray as the region enclosed in Fig. 3(d). In addition to preserving the original trimer mode, now written with four components as $\{+, 0, -, 0\}$, an extra mode appears with the same frequency $\beta = 0$. This mode has a profile $\{+, 0, 0, -V_1/V_2\}$ or $\{0, 0, +, -V_1/V_2\}$, where always the center site of the original three-site miniarray remains zero. In fact, this new mode does not change our criterion for constructing FB systems. It tells us that the original three-site miniarray was not enough to describe the new quasi-1D composed system, so we may consider a larger miniarray structure (although it allowed the generation of a 3D FB spinelike ribbon lattice as noted above).

Now, by connecting several three-site miniarrays using several connector sites, we are able to construct a full cross lattice, as shown in Fig. 3(d). We define the unitary cell of this lattice [enclosed area in Fig. 3(d)] and solve the eigenvalue problem (2), finding that

$$\beta(k_x) = 0, 0, \pm \sqrt{4V_2^2 \cos^2(k_x) + 2V_1^2}.$$

We plot these four bands in Fig. 3(e). We find two dispersive and two degenerated flat ($\beta = 0$) bands. These zero-dispersion bands are composed of the localized states shown in Fig. 3(c), exactly the same obtained for the miniarray and for the composed small system [Fig. 3(b)].

B. Sawtooth lattice

We continue using the modes of the trimer miniarray, but this time we focus on the third one: $\{-, \sqrt{2}, -\}$ [see Fig. 4(a)]. We add a connector site and couple a second three-site miniarray, as shown in Fig. 4(b). As the coupling coefficient depends on the geometry, we allow the new system

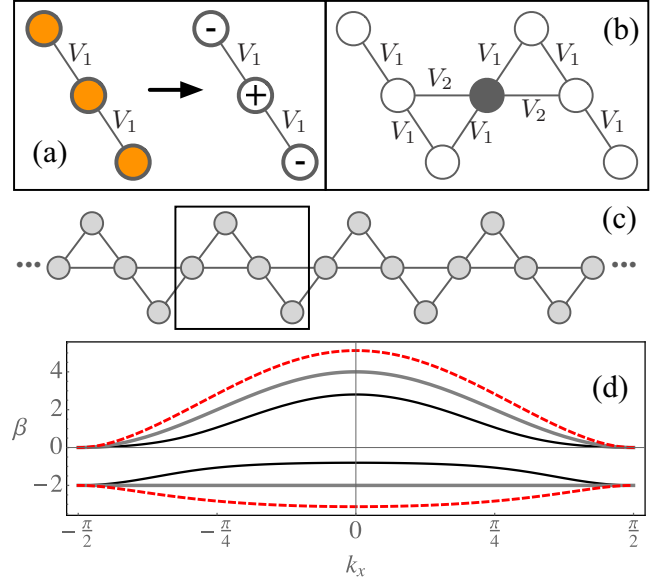


FIG. 4. (a) Three-site miniarray and one of its linear modes. (b) Two miniarrays connected by a connector (dark) site. (c) Sawtooth lattice. (d) Linear spectrum for $\delta = 0.75$ (thin), $\sqrt{2}$ (thick), and 2 (dashed).

to have diagonal (V_1) and horizontal (V_2), in principle different, coupling coefficients. By injecting the $\{-, \sqrt{2}, -\}$ mode in the first miniarray, we realize that an extra condition may be satisfied. If we write the stationary equation (2) for the connector site amplitude, we get

$$\beta \cdot \psi_C = V_1 \cdot (0 - A) + V_2(\sqrt{2}A + 0) = (V_2\sqrt{2} - V_1)A.$$

Therefore, in order to have a zero amplitude at the connector site, a ratio $\delta \equiv V_1/V_2 = \sqrt{2}$ is required. For this particular condition, the third mode of the three-site miniarray becomes a mode of the composed system as well. In fact, it can be located in three different positions in this new composed system, because the connector site forms also a similar miniarray with a different inclination.

By continuing to add miniarrays via connector sites, we are able to construct a full sawtooth lattice like the one sketched in Fig. 4(c), where the unitary cell of four sites is demarcated by an enclosed area. However, due to the sawtooth symmetry, the four sites can be reduced to just two sites [19]. We solve the eigenvalue problem (2) with this geometry and find two linear bands

$$\beta(k_x) = V_2[\cos(2k_x) \pm f(k_x, \delta)],$$

where $f(k_x, \delta) = \sqrt{1 + 4(\delta^2 - 1)\cos^2(k_x) + 4\cos^4(k_x)}$. If $\delta = \sqrt{2}$, the two bands reduce to $\beta(k_x) = -2V_2$ and $4V_2 \cos^2(k_x)$, i.e., a flat band emerges for this particular ratio between coupling coefficients. In fact, this is exactly the same condition for the third mode to be a mode of the composed system. Therefore, the $\{-, \sqrt{2}, -\}$ mode is also a mode of a full sawtooth lattice, when satisfying the condition $\delta = \sqrt{2}$. In Fig. 4(d) we show the linear spectrum for three different values of δ , where we observe that the lower band becomes completely flat at this particular condition.

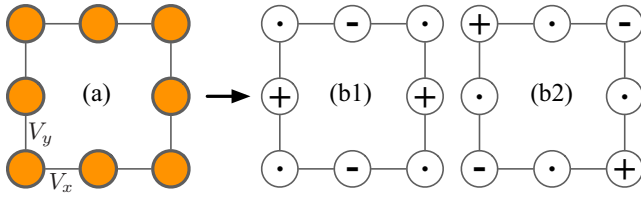


FIG. 5. (a) Eight-site miniarray. (b) Two linear modes.

V. TWO-DIMENSIONAL LIEB-LIKE EXAMPLES

Now we review our method for two-dimensional Lieb FB lattices, which have received a great deal of attention recently [22,23,26,33,35]. We start by identifying the miniarray necessary to construct a standard Lieb lattice. In Fig. 5(a) we show a miniarray example consisting of eight sites forming a ring, including an anisotropy ($V_x \neq V_y$) degree of freedom. This system possesses eight linear modes, but we consider only two for our study: $\{0, +, 0, -V_y/V_x, -V_y/V_x, 0, +, 0\}$ [Fig. 5(b1)] and $\{-, 0, +, 0, 0, +, 0, -\}$ [Fig. 5(b2)]. These two modes are degenerated with a frequency $\beta = 0$, due to a perfect cancellation of phases.

A. Lieb lattice

We construct a Lieb 2D lattice by using the miniarray and first mode shown in Figs. 5(a) and 5(b1), respectively. In this case, a zero site of the miniarray is used as a connector site (there is no need to add an extra site, although when doing it a

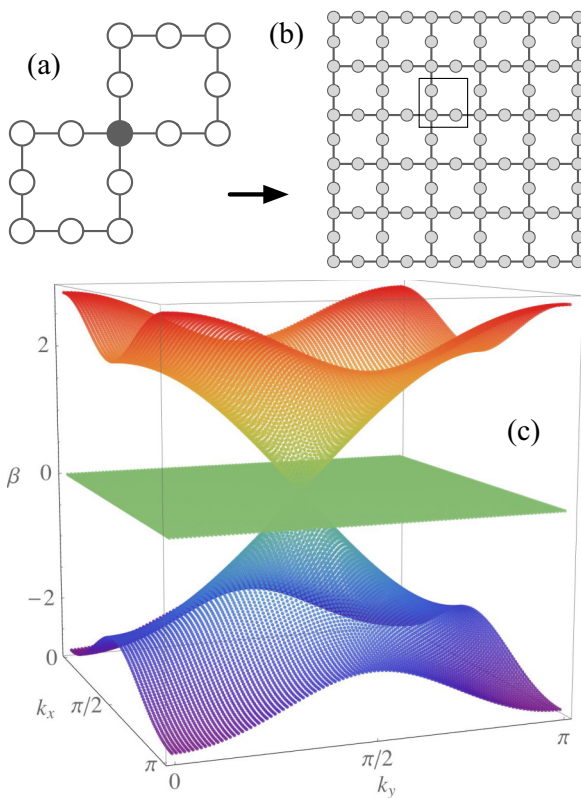


FIG. 6. (a) Two miniarrays connected by a connector (dark) site. (b) Lieb lattice. (c) Linear spectrum for $V_x = V_y = 1$.

different FB lattice could be created, as we will show below). Figure 6(a) shows a composed system formed using the connection of two miniarrays sharing the same connector site at one corner. As expected, the $\{0, +, 0, -V_y/V_x, -V_y/V_x, 0, +, 0\}$ mode is also a solution of this composed system in either of the two miniarrays, due to the perfect phase cancellation at the corner sites. By repeating this procedure in different directions and using different corner sites, we are able to construct a full 2D Lieb lattice as shown in Fig. 6(b). The original miniarray mode can be located in different miniarrays of the full lattice, all of them degenerated with $\beta = 0$.

Solving Eq. (2) for this lattice geometry, which consider three sites per unit cell [see enclosed region in Fig. 6(b)], we find the corresponding linear spectrum

$$\beta(k_x, k_y) = 0, \pm 2\sqrt{V_x^2 \cos^2(k_x) + V_y^2 \cos^2(k_y)}.$$

As it is expected from our method, the degenerated miniarray modes form a complete zero-dispersion band at $\beta = 0$ [see Fig. 6(c)]. Two dispersive bands are found for this system as well [22,23].

B. Lieb 2 lattice

We construct a Lieb 2 lattice by using the miniarray and second mode shown in Figs. 5(a) and 5(b2), respectively. For this problem, we have zero-amplitude sites at the sides of the miniarray. So we add a new connector site to connect this miniarray to another one, as shown in the example presented in Fig. 7(a). If we inject the original stationary $\{-, 0, +, 0, 0, +, 0, -\}$ mode [Fig. 5(b2)] in one or both miniarrays, it will also be a solution of the composed system, because the connector site remains zero. Naturally, we can add several connector sites on the four sides of the original miniarray and connect more miniarrays in different directions. In this way, we are able to compose a full new system that we refer to as a Lieb 2 lattice, with the geometry shown in Fig. 7(b). This composed system possesses ten sites per unit cell [see enclosed region in Fig. 7(b)] and therefore a linear spectrum having ten linear bands. The analytical form of these bands is not trivial, so we only present their plot in Fig. 7(c). By inspecting the spectrum, we find two flat bands, both located at $\beta = 0$. The first one is composed of $\{-, 0, +, 0, 0, +, 0, -\}$ miniarray modes, which continue being solutions of the extended system [see the shaded area at the bottom left corner of Fig. 7(b)]. Additionally, a new localized FB state appears in the region in between four miniarrays. It has eight sites different from zero in a staggered sign sequence, which is necessary to cancel the transport to the rest of the lattice [see the bottom right shaded region in Fig. 7(b)]. For an isotropic configuration ($V_x = V_y$), all amplitudes have equal magnitude. However, for anisotropic lattices ($V_x \neq V_y$) the relation of amplitudes becomes a bit more complicated. If we define the horizontal connector site amplitude as C , the vertical connector site amplitude as B , and the corner site amplitude as A , then $C = -V_y A / V_x$ and $B = -V_x A / V_y$. Similar to the cross lattice case (Fig. 3), the appearance of this new localized state does not change our method, it only implies that the initial miniarray was not enough to describe the full new composed system.

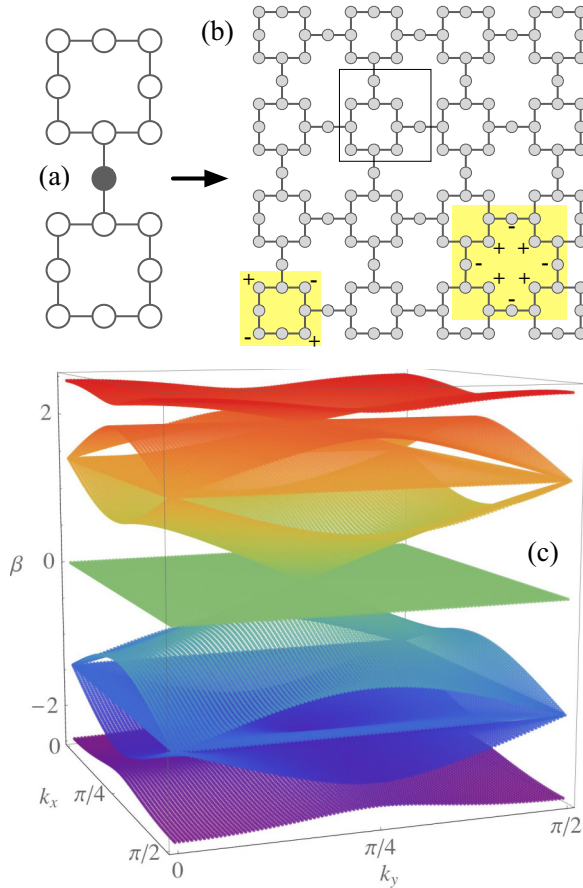


FIG. 7. (a) Two miniarrays connected by a connector (dark) site. (b) Lieb 2 lattice. (c) Linear spectrum for $V_x = V_y = 1$.

VI. MULTIPLE FLAT BANDS

The number of FBs of a given lattice depends on the number of stationary modes that satisfy the symmetry condition at the connector sites of a given miniarray. Therefore, by analyzing the specific geometry, we can construct different lattices having more than only one FB. For example, the cross and the Lieb 2 lattices present two FBs at frequency $\beta = 0$. As we discussed before, the modes belonging to these two bands are spatially different, but both preserve the condition of having a zero amplitude at the connector sites, as the original miniarray mode does. Therefore, depending on the geometry and complexity of a given miniarray, it is possible to find additional compact linear modes that are also solutions of the small system and that preserve the condition of canceling the transport at the same connector site.

Now we show explicitly how to construct a system possessing more than one flat band. We focus on a simple system, the so-called B2-ribbon. In Fig. 8(a), left, we show a four-site miniarray that possesses four linear modes, with three of them being useful for FB lattice composition. If we think of an horizontally oriented ribbon lattice, the two good modes (useful for phase cancellation) are the ones shown in Fig. 8(a), right. These modes are denoted by $\{-, +, -, +\}$ and $\{-, +, +, -\}$, with frequencies $\beta = (V_x - V_y)$ and $\beta = -(V_x + V_y)$, respectively. We immediately observe that when connecting two miniarrays via a connector site [as shown in

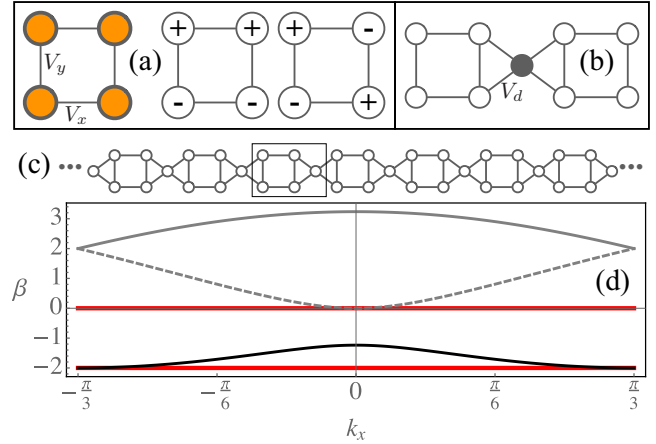


FIG. 8. (a) Four-site miniarray and two of their linear modes. (b) Two miniarrays connected by a connector (dark) site. (c) B2-ribbon lattice. (d) Linear spectrum for $V_x = V_y = V_d = 1$.

Fig. 8(b)], the dynamical equation for this site will be just zero, when initializing the system with one of these stationary modes (the connector site is symmetrically coupled to the miniarrays with a coefficient V_d). By increasing the system size with more connectors and more miniarrays, we are able to construct a full B2-ribbon lattice [see Fig. 8(c)]. We compute the linear spectrum of this extended system by identifying the unitary cell of this lattice [enclosed region in Fig. 8(c)]. This cell contains five sites, therefore five linear bands are generated as Fig. 8(d) shows. The analytical expressions for the three dispersive bands are not compact and we will not write them explicitly. The two zero-dispersion bands are simply located at frequencies $\beta = (V_x - V_y)$ and $\beta = -(V_x + V_y)$, exactly at the same frequencies as the original miniarray modes. Therefore, as expected, these two modes are also localized solutions for the extended system and generate two full flat bands.

This example is one of the many possible configurations useful to create lattices presenting more than one FB. Of course, this method could also be extended to full 2D lattices and not only to quasi-1D ribbons. In fact, the lattice Lieb 2 (see Fig. 7) is an example of this. In general, the dimension is not important; the key point is to preserve the discreteness of the system that allows the cancellation of phases for the modes of the miniarray and therefore the cancellation of transport across the lattice.

VII. ADDITIONAL CONSIDERATIONS

A. Aperiodic composition

It is possible to construct aperiodic lattices by connecting different miniarrays via connector sites. The particular mode of every miniarray will also be a mode of the full lattice and could form a dense band, of course depending on its particular frequency. This point is very interesting because aperiodic systems will present no dispersive bands at all, but could present full FBs composed of different states. Therefore, the disorder could promote localization in the form of destructive interference of plane waves (Anderson localization [4,5]) or

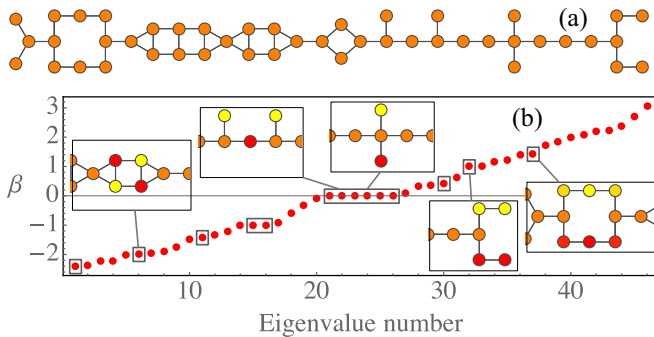


FIG. 9. (a) Composed aperiodic system and its (b) linear spectrum. Insets in (b) show the amplitude profile for some localized modes of this system (the color scale increases from red to yellow, with orange being equal to zero).

due to a local geometric phase cancellation (FB localization [16,22,23]). As our criterion does not depend on the periodicity but on the discreteness of the system (miniarray geometry), we can compose an aperiodic system as a sequence of different miniarrays connected by several connector sites. This system will not be periodic, but still will preserve all the properties of the different coupled miniarrays. In Fig. 9(a) we show an example of a small composed system, which includes eight different miniarrays. We obtain its linear spectrum by numerically diagonalizing the corresponding coupling matrix V_{nm} and plot β versus the eigenvalue number in Fig. 9(b). As this system is not periodic, its spectrum does not form a soft curve [36]. Additionally, we realize that all the miniarray modes [14 in this case; see the boxes in Fig. 9(b)] that satisfy the condition for having a zero amplitude at a given connector site are also a solution of this extended system. This array is clearly aperiodic, but can be extended to form a periodic lattice by repeating the same pattern several times. By doing this, we would generate a new periodic system, but having a more complex unitary cell [Fig. 9(a)]. Therefore, the original miniarray states will also be a solution of the extended system and will form 14 different degenerated flat bands.

B. Next-nearest-neighbor coupling

Not all the lattices preserve their zero-dispersion band when including next-nearest-neighbor interactions. For example, a Lieb lattice adds curvature to the original flat band when including diagonal coupling [37] and the FB localized modes are simply lost. However, this is not an intrinsic problem of FB systems, the point is that the lattice geometry is just not the right one. In order to construct a lattice with a FB, which is robust against next-nearest-neighbor interactions, there is no need to add any new ingredient to our method. We just may choose the right geometrical configuration for connector sites to ensure that when considering, for example, a diagonal coupling, the dynamical equation for the connector site continues being zero, when injecting a FB mode as an initial condition. For example, this occurs for the previous Lieb 2 lattice [Fig. 7(b)]. As we explained before, this lattice possesses two FBs at $\beta = 0$. When including diagonal coupling coefficients, both FBs survive, but one of them shifts to a frequency $\beta = -2V_d$, where V_d corresponds to

the next-nearest coefficient (we can see that when $V_d = 0$, the band converges to its previous location). Another example is the B2-ribbon lattice (Fig. 8). When including a diagonal interaction between vertices of the miniarray, the $\{-, +, -, +\}$ and $\{-, +, +, -\}$ modes shift their frequencies to $\beta = (V_x - V_y) - V_d$ and $\beta = -(V_x + V_y) + V_d$, respectively. Therefore, the FBs also shift their frequencies to these values and the mode profiles preserve their perfect localization.

C. Anisotropy

In typical photonics setups, the anisotropy of crystals or of the waveguide modes is an important parameter to be taken into account when studying the linear properties of a given lattice. For example, in femtosecond written waveguide arrays [22,35], the coupling interaction strongly depends on the elliptical profile of written waveguides (although the silica buffer is essentially isotropic). On the other hand, photonic lattices induced in SBN photorefractive crystals [21,26] also presents a strong anisotropy, but caused by the crystal itself (induced waveguides have a symmetrical profile). This consideration effectively implies that, for a fixed distance, the coupling also changes depending on its orientation ($V_x \neq V_y$) [32]. When computing the linear spectrum of a given lattice, the anisotropy could destroy the flatness of a previous flat band. For example, a kagome lattice has no FB when horizontal coupling differ from the diagonal one [21]. However, there are several systems where this effect does not affect at all the flatness of the band, for example, the cross or the Lieb lattices.

We already considered the anisotropy in our method from the very beginning and we were able to construct robust systems presenting FBs. The only necessary condition is to have a balance between the mode amplitudes in terms of the different coupling interactions of the system. This essentially implies that the amplitude of FB modes will not have the same value at different positions. The most important consideration is that the connector dynamical equation must be zero from the beginning, when injecting a given miniarray mode. An interesting example is the Lieb 2 lattice. This system has two FBs at $\beta = 0$. The first one is composed of localized modes having only four sites with amplitude different from zero [bottom left corner in Fig. 7(c)]. As we can see, the cancellation of phases for this mode is always horizontal or vertical, therefore the anisotropy balance is not required and modes simply have equal amplitudes but different phases. On the other hand, the second flat band is composed of modes that cancel the transport by balancing vertical and horizontal interactions [bottom right corner in Fig. 7(c)]. Therefore, a correction of amplitudes is required depending on a given anisotropy $V_x \neq V_y$, as we explicitly described before.

If we consider that different sites of the unitary cell could present different propagation constants (determined by $\epsilon_{\vec{n}}$), an effective anisotropy is generated in the system. Again, this is not a problem for the generation of FB lattices, however extra conditions for the balance of equations need to be fulfilled. Essentially, by starting from a given miniarray with a defined configuration of $\epsilon_{\vec{n}}$, new modes need to be computed. Then, by inspecting their symmetry one can realize if these modes are good candidates for spatial localization on an extended lattice. If the required balance is not achieved when the propagation

constants are different, the coupling anisotropy could help solve this. However, this overall balance could be too complex to be implemented in real experiments.

D. Nonlinear solutions

One of the most common nonlinear interactions studied in diverse lattice systems corresponds to a cubic nonlinearity [2,12]. In optics this interaction arises from the Kerr effect, which is nothing but an increment of the refractive index due to the intensity of a given beam. In Bose-Einstein condensates, this interaction originates from the scattering between particles and in solid-state physics from the interaction, for example, between phonons and electrons on a given lattice. In model (1), this nonlinear effect can be included by adding a term $\gamma |\psi_{\vec{n}}|^2 \psi_{\vec{n}}$, where γ corresponds to the strength of the nonlinear response. When looking for real solutions, the stationary problem to solve becomes simply

$$\beta(\vec{k})A_{\vec{n}} = \sum_{\vec{m} \neq \vec{n}} V_{\vec{n},\vec{m}} A_{\vec{m}} e^{i\vec{k} \cdot (\vec{m} - \vec{n})} + \gamma A_{\vec{n}}^2 A_{\vec{n}}.$$

In general, any FB mode possessing a set of N amplitudes A , but with alternating signs, has a very simple and compact form [38,39]. As the connector sites amplitudes remain zero, the total power, defined as $P = \sum_{\vec{n}} |A_{\vec{n}}|^2$, is just given by $P = NA^2$. The frequency of the nonlinear solution becomes $\beta = \beta_0 + \gamma A^2$ (where the frequency shift β_0 depends on the specific FB of a given lattice) and therefore a very simple and exact relation between the frequency and power arises

$$P = \frac{N}{\gamma} (\beta - \beta_0).$$

These nonlinear solutions are perfectly localized in a very compact spatial region. They are analytical compacton solutions [40,41], which conserve their spatial profile in the whole range of parameters. They bifurcate at the FB position ($\beta = \beta_0$) for a zero level of power ($P = 0$). These solutions exist for positive and negative nonlinearity, with the corresponding shift on the sign frequency to ensure that $P > 0$.

When the FB modes possess a more complex spatial profile, including differences in the magnitude of the amplitudes, a more complicated relation is required. For example, in linear sawtooth lattices the FB exists for a very specific value of coupling coefficients. Additionally, the FB mode has a nonsymmetric profile of the form $\{\dots, 0, -1, \sqrt{2}, -1, 0, \dots\}$. Therefore, when increasing the solutions power, the amplitudes will change and the perfect balance will be more tricky. Reference [42] explores how to preserve this balance in a nonlinear context (cubic and saturable), but allowing the system to also modify the coupling constants.

E. Continuous model

Finally, we study the robustness of our method in a more realistic environment. Although discrete models, based on nearest-neighbor interactions, describe very well the phenomenology observed in direct experiments [2,12], a better proof of the stable propagation of localized FB modes is

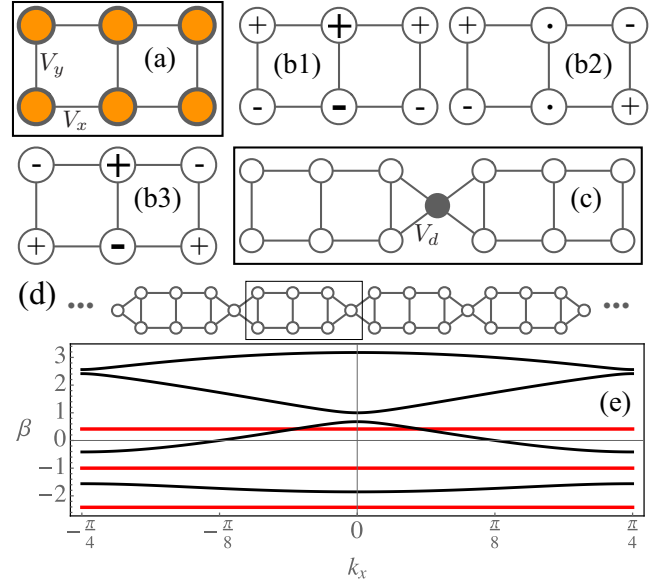


FIG. 10. (a) Six-site miniarray and (b) three of their linear modes. (c) Two miniarrays connected by a connector (dark) site. (d) B3-ribbon lattice. (e) Linear spectrum for $V_x = V_y = V_d = 1$.

obtained by numerically solving a paraxial wave equation

$$-i \frac{\partial \psi}{\partial z} = \frac{1}{2k_0 n_0} \nabla_{\perp}^2 \psi + k_0 \Delta n(x, y) \psi. \quad (3)$$

Here $\psi = \psi(x, y, z)$ describes the envelope of the electric field, z is the propagation coordinate, $k_0 = 2\pi/\lambda$ corresponds to the wave number in free space, λ is the vacuum wavelength, and n_0 is the refractive index of the bulk material. The function $\Delta n(x, y)$ defines the refractive index structure, which depends on the specific lattice geometry. This function indicates the transversal variations of the refractive index, showing a larger value at the center of waveguide positions. In addition, $\nabla_{\perp}^2 = \partial_x^2 + \partial_y^2$ corresponds to the transverse Laplacian operator.

As an interesting example we study a system possessing three FBs, as shown in Fig. 10. A six-site miniarray [Fig. 10(a)] has three FB modes [Fig. 10(b)] that cancel the amplitude at the connector site [Fig. 10(c)]. The frequencies of these modes are $-V_y + \sqrt{2}V_x$, $-V_y$, and $-V_y - \sqrt{2}V_x$, respectively. When computing the linear spectrum [considering the unitary cell shown in Fig. 10(d)], we find seven linear bands [see Fig. 10(e)]. Four of them are dispersive and three are completely flat. The frequencies of the zero-dispersion bands are exactly the same as the ones of the miniarray modes shown in Fig. 10(b), as expected from our method.

To study this lattice in a more realistic configuration, we set the lattice geometry in the model (3) by defining the function $\Delta n(x, y)$ [22]. We assume elliptical waveguides [8], which induces a strong effective anisotropy $V_y \neq V_x$. This does not affect the flatness of the three degenerated bands; it only implies a different balance between the FB modes amplitudes. Considering standard parameters used in Ref. [22] ($n_0 = 1.40$, a lattice period of $d = 20 \mu\text{m}$, a propagation distance of $L = 10 \text{ cm}$, $\lambda = 532 \text{ nm}$, and a maximum index contrast of 0.67×10^{-3}), we implement a standard beam propagation method to solve Eq. (3) numerically.

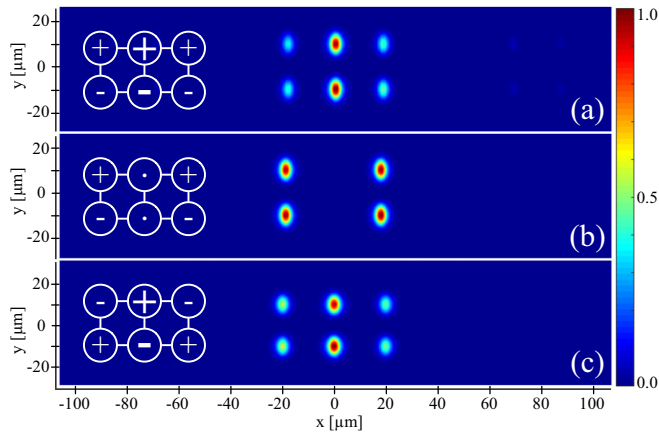


FIG. 11. Transversal intensity profile $|\psi(x, y, L)|^2$, after propagating a distance $L = 10$ cm, in a B3-ribbon lattice geometry. (a)–(c) Different output profiles for the input conditions sketched in each figure. Density plots are normalized to one, as indicated by the color map.

In Fig. 11 we show our results for three different input conditions. We observe that the three input profiles, corresponding to the three FB modes of a B3-ribbon lattice [see Fig. 10(b)], propagate a distance of 10 cm without suffering noticeable distortion. In fact, Fig. 11(a) shows the excitation of some outsider lobes, which are very weak in comparison to the central highly excited sites. In Figs. 11(b) and 11(c) only the mode profiles are observable, with essentially a zero background. This result is certainly very interesting because we are using discrete solutions as input conditions of a continuous model. It is well known that a discrete (tight-binding) model describes only the lower part of the spectrum of an, in principle, infinite band-gap system [1]. When thinking of corrections to the nearest-neighbors model (1), the first consideration to have in mind is diagonal or next-nearest-neighbor interactions. The flat band on a B3-ribbon lattice example are robust against anisotropy and also second-order linear interactions. This is a

good indication that the discrete predictions will be observable for long distances in a continuous (realistic) medium. However, as this is an approximation of a more complex system, which includes an infinite set of linear bands, after even longer distances the FB states may start to experience diffraction across the lattice.

VIII. CONCLUSION

In this work we developed a simple method to construct different FB lattices. By inspecting the miniarray mode profiles, we identified the good candidate modes for canceling the transport across a full lattice, as a consequence of a local geometric phase cancellation at the connector sites. Our method is based on the discrete properties of a given lattice and the right identification of the corresponding miniarray. In this way, our method is able to explain all the already known FB lattice systems, but also give a simple recipe for inventing new ones. As our technique is based on the modes of a given miniarray, the lattice composition method will always give a complete FB, composed of spatially localized linear modes. By allowing the system to have extra interactions, we can also find robust lattices that preserve the localization of FB modes when including, for example, next-nearest-neighbor interactions. This becomes very important when studying the lattice phenomenology experimentally, as we showed by numerically solving a continuous model. Finally, we showed that some nonlinear FB lattices possess simple analytical compact solutions, which could be relevant when thinking of the mobility of strongly localized wave packets [38].

ACKNOWLEDGMENTS

The authors acknowledge useful discussions with C. Cantillano and B. Real. This work was supported in part by Programa ICM Grant No. RC-130001 and FONDECYT Grant No. 1151444.

-
- [1] C. Kittel, *Introduction to Solid State Physics*, 7th ed. (Wiley, New York, 1996).
- [2] F. Lederer, G. I. Stegeman, D. N. Christodoulides, G. Assanto, M. Segev, and Y. Silberberg, Discrete solitons in optics, *Phys. Rep.* **463**, 1 (2008).
- [3] P. W. Anderson, *Phys. Rev.* **109**, 1492 (1958).
- [4] T. Schwartz, G. Bartal, S. Fishman, and M. Segev, *Nature (London)* **446**, 52 (2007).
- [5] Y. Lahini, A. Avidan, F. Pozzi, M. Sorel, R. Morandotti, D. N. Christodoulides, and Y. Silberberg, *Phys. Rev. Lett.* **100**, 013906 (2008).
- [6] H. S. Eisenberg, Y. Silberberg, R. Morandotti, A. R. Boyd, and J. S. Aitchison, *Phys. Rev. Lett.* **81**, 3383 (1998).
- [7] J. W. Fleischer, T. Carmon, M. Segev, N. K. Efremidis, and D. N. Christodoulides, *Phys. Rev. Lett.* **90**, 023902 (2003).
- [8] A. Szameit, D. Blömer, J. Burghoff, T. Schreiber, T. Pertsch, S. Nolte, A. Tünnermann, and F. Lederer, *Opt. Express* **13**, 10552 (2005).
- [9] J. W. Fleischer, M. Segev, N. K. Efremidis, and D. N. Christodoulides, *Nature (London)* **422**, 147 (2003).
- [10] A. Szameit, J. Burghoff, T. Schreiber, T. Pertsch, S. Nolte, A. Tünnermann, and F. Lederer, *Opt. Express* **14**, 6055 (2006).
- [11] D. K. Campbell, S. Flach, and Y. S. Kivshar, *Phys. Today* **57**(1), 43 (2004).
- [12] S. Flach and A. Gorbach, *Phys. Rep.* **467**, 1 (2008).
- [13] F. Fedele, J. Yang, and Z. Chen, *Opt. Lett.* **30**, 1506 (2005).
- [14] I. Makasyuk, Z. Chen, and J. Yang, *Phys. Rev. Lett.* **96**, 223903 (2006).
- [15] L. B. Soldano and E. C. M. Pennings, *J. Lightwave Technol.* **13**, 615 (1995).
- [16] S. Mukherjee and R. R. Thomson, *Opt. Lett.* **40**, 5443 (2015).
- [17] F. Baboux, L. Ge, T. Jacqmin, M. Biondi, A. Lemaître, L. Le Gratiet, I. Sagnes, S. Schmidt, H. E. Türeci, A. Amo, and J. Bloch, *Phys. Rev. Lett.* **116**, 066402 (2016).
- [18] T. Zhang and G.-B. Jo, *Sci. Rep.* **5**, 16044 (2015).

- [19] S. Weimann, L. Morales-Inostroza, B. Real, C. Cantillano, A. Szameit, and R. A. Vicencio, *Opt. Lett.* **41**, 2414 (2016).
- [20] S. A. Parameswaran, I. Kimchi, A. M. Turner, D. M. Stamper-Kurn, and A. Vishwanath, *Phys. Rev. Lett.* **110**, 125301 (2013).
- [21] Y. Zong, S. Xia, L. Tang, D. Song, Y. Hu, Y. Pei, J. Su, Y. Li, and Z. Chen, *Opt. Express* **24**, 8877 (2016).
- [22] R. A. Vicencio, C. Cantillano, L. Morales-Inostroza, B. Real, C. Mejía-Cortés, S. Weimann, A. Szameit, and M. I. Molina, *Phys. Rev. Lett.* **114**, 245503 (2015).
- [23] S. Mukherjee, A. Spracklen, D. Choudhury, N. Goldman, P. Öhberg, E. Andersson, and R. R. Thomson, *Phys. Rev. Lett.* **114**, 245504 (2015).
- [24] S. Taie, H. Ozawa, T. Ichinose, T. Nishio, S. Nakajima, Shuta, and Y. Takahashi, *Sci. Adv.* **1**, e1500854 (2015).
- [25] R. A. Vicencio and C. Mejía-Cortés, *J. Opt.* **16**, 015706 (2014).
- [26] S. Xia, Y. Hu, D. Song, Y. Zong, L. Tang, and Z. Chen, *Opt. Lett.* **41**, 1435 (2016).
- [27] S. Deng, A. Simon, and J. Köhler, *J. Solid State Chem.* **176**, 412 (2003).
- [28] S. Miyahara, K. Kubo, H. Ono, Y. Shimomura, and N. Furukawa, *J. Phys. Soc. Jpn.* **74**, 1918 (2005).
- [29] D. L. Bergman, C. Wu, and L. Balents, *Phys. Rev. B* **78**, 125104 (2008).
- [30] S. Flach, D. Leykam, J. D. Bodyfelt, P. Matthies, and A. S. Desyatnikov, *Eur. Phys. Lett.* **105**, 30001 (2014).
- [31] M. Hyrkäs, V. Apaja, and M. Manninen, *Phys. Rev. A* **87**, 023614 (2013).
- [32] A. Szameit, F. Dreisow, T. Pertsch, S. Nolte, and A. Tünnermann, *Opt. Exp.* **15**, 1579 (2007).
- [33] F. Diebel, D. Leykam, S. Kroesen, C. Denz, and A. S. Desyatnikov, *Phys. Rev. Lett.* **116**, 183902 (2016).
- [34] R. Keil, C. Poli, M. Heinrich, J. Arkininstall, G. Weihs, H. Schomerus, and A. Szameit, *Phys. Rev. Lett.* **116**, 213901 (2016).
- [35] D. Guzmán-Silva, C. Mejía-Cortés, M. A. Bandres, M. C. Rechtsman, S. Weimann, S. Nolte, M. Segev, A. Szameit, and R. A. Vicencio, *New J. Phys.* **16**, 063061 (2014).
- [36] R. A. Vicencio and S. Flach, *Phys. Rev. E* **79**, 016217 (2009).
- [37] D. Leykam, O. Bahat-Treidel, and A. S. Desyatnikov, *Phys. Rev. A* **86**, 031805(R) (2012).
- [38] R. A. Vicencio and M. Johansson, *Phys. Rev. A* **87**, 061803(R) (2013).
- [39] P. P. Beličev, G. Glirorić, A. Radosavljević, A. Maluckov, M. Stepčić, R. A. Vicencio, and M. Johansson, *Phys. Rev. E* **92**, 052916 (2015).
- [40] P. G. Kevrekidis and V. V. Konotop, *Phys. Rev. E* **65**, 066614 (2002).
- [41] P. G. Kevrekidis, V. V. Konotop, A. R. Bishop, and S. Takeno, *J. Phys. A* **35**, L641 (2002).
- [42] M. Johansson, U. Naether, and R. A. Vicencio, *Phys. Rev. E* **92**, 032912 (2015).